

Radial Electric Field Profiles in JET Advanced Tokamak Scenarios with Toroidal Field Ripple

K. Crombé¹, Y. Andrew², T.M. Biewer³, E. Blanco⁴, P. de Vries², C. Giroud², N. C. Hawkes²,
A. Meigs², T. Tala⁵, M. von Hellermann⁶, K.-D. Zastrow² and JET-EFDA contributors*

JET-EFDA, Culham Science Centre, OX14 3DB, Abingdon, UK

¹Department of Applied Physics, Ghent University, Rozier 44, B-9000 Gent, Belgium

²EURATOM/UKAEA Fusion Association, Culham Science Centre, Oxon. OX14 3DB. UK

³Oak Ridge National Laboratory, Oak Ridge, TN 37831-6169, Tennessee, USA

⁴Laboratorio Nacional de Fusion, Asociacion EURATOM-CIEMAT, Madrid, Spain

⁵Association EURATOM-Tekes, VTT, P.O. Box 1000, FIN-02044 VTT, Finland

⁶FOM Institute for Plasma Physics Rijnhuizen, Association EURATOM-FOM, Trilateral Euregio
Cluster, P.O. Box 1207, 3430 BE Nieuwegein, The Netherlands

* See Appendix of M.L. Watkins et al., Fusion Energy 2006 (Proc. 21st Int. Conf. Chengdu, 2006) IAEA, (2006)

INTRODUCTION

Toroidal Field (TF) ripple has been shown to affect the toroidal rotation velocity (v_ϕ) profiles in tokamaks through enhanced losses of fast and thermal ions [1, 2]. The ripple amplitude (δ) is defined as the relative variation of the magnetic field at the separatrix. For standard JET plasmas $\delta = 0.08\%$, while for ITER it will be of the order of $\delta = 0.5\%$. Experiments were performed on JET to study the formation and sustainment of Internal Transport Barriers (ITBs) in the presence of TF ripple [3]. Poloidal rotation velocities (v_θ) are presented in ITB plasmas with gradually increasing δ and are used to calculate radial electric field (E_r) profiles.

EXPERIMENTAL RESULTS

Two sets of discharges are presented for which the ripple amplitude was gradually increased, indicated in table 1. In one set Lower Hybrid Current Drive (LHCD) was used during the current ramp-up to create a radial zone with strongly negative magnetic shear, the reversed shear (RS) scenario, while the second set did not have LHCD and the q -profile is monotonic or weakly reversed, the optimised shear (OS) scenario. The RS plasmas were run with $B_t/I_p = 2.2\text{T}/1.8\text{MA}$ and the OS plasmas with $B_t/I_p = 2.2\text{T}/1.9\text{MA}$. The Neutral Beam heating (NBI) varied between 10.0MW and 13.2MW and between 3.0MW and 3.8MW of off-axis Ion Cyclotron Resonant Frequency

Shot	δ [%]	ρ_{Ti}^*	t_1 [s]	t_2 [s]
RS				
69670	0.08	0.040	4.725	5.725
69665	0.63	0.039	5.525	6.025
69684	0.82	0.026	4.375	6.275
69690	1.00	0.024	4.125	5.675
OS				
69676	0.08	0.028	4.375	5.125
69677	0.63	0.029	4.375	5.225
69682	0.82	0.024	4.475	4.875
69679	1.00	0.023	4.325	4.875

presented for which the ripple amplitude was gradually increased, indicated in table 1. Current Drive (LHCD) was up to create a radial zone with shear, the reversed shear (RS) scenario. The RS plasmas did not have LHCD and the weakly reversed, the OS scenario. The OS plasmas were run with $B_t/I_p = 2.2\text{T}/1.8\text{MA}$ and the OS plasmas with $B_t/I_p = 2.2\text{T}/1.9\text{MA}$. The Neutral Beam heating (NBI) varied between 10.0MW and 13.2MW and between 3.0MW and 3.8MW of off-axis Ion Cyclotron Resonant Frequency

heating (ICRH) was applied at 37MHz with pi/2 phasing. The profiles on the left hand side of fig. 1 (a,c,e) are for a time t_1 (given in table 1) between 50 and 500 ms before the start of the

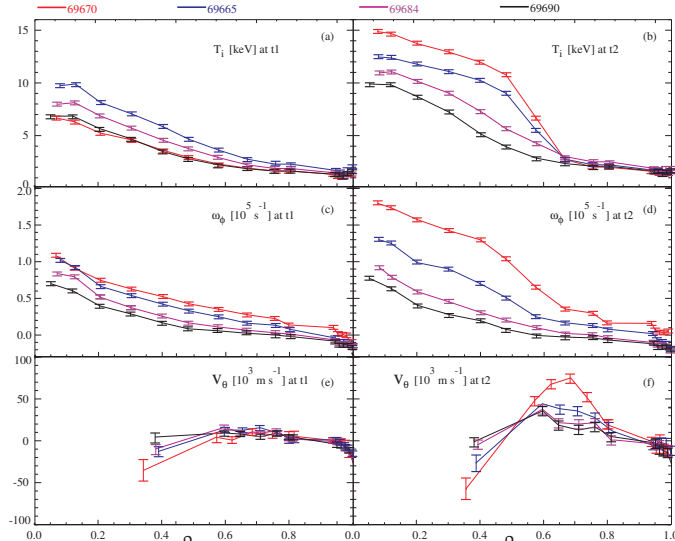


Figure 1: (a-b) ion temperature, (c-d) toroidal and (e-f) poloidal rotation velocity for the series of four RS shots with different ripple amplitude, before the start of the ITB on the left hand side, and around the maximum of the ITB strength on the right hand side for the times indicated in table 1

ITB (during the phase when T_i , v_ϕ and v_θ show little variation). The start of the ITB is defined as when $\rho^*_{T_i}$ exceeds the empirical value for JET of 0.014 [4]. The profiles on the right hand side (b,d,f) are for a time t_2 around the maximum of the ITB strength (the largest $\rho^*_{T_i}$ value that was achieved during the pulse). Figures 1 (a) and (b) show T_i , (c) and (d) v_ϕ and (e) and (f) v_θ , combining the data from

the core and edge CXRS diagnostics [5,6]. The highest central T_i is 15 keV and is reached for shot no. 69670, with the standard JET ripple $\delta=0.08\%$. It can be seen that v_ϕ is strongly affected by increasing δ [2]; in the pre-ITB phase an edge zone of about 7 cm width in counter rotation is observed for ripple amplitude $\delta =0.63\%$, extending from the scrape-off-layer inwards up to $\rho = 0.87$. For $\delta =1.00\%$ this zone extends up to $\rho =0.70$ and is 20 cm wide. The barrier strength decreases with increasing ripple. The poloidal rotation velocity at $\rho = 0.30$ is between 3 and -35 km/s at t_1 , i.e. prior to when the ITB criterion is exceeded. This value is obtained early on during the main heating phase and remains at the same level for several seconds. No sign of a transient spin-up just before the start of the ITB is measured with the present time resolution of the diagnostic at 50ms. An increase to a maximum of -60 km/s is seen at t_2 , well into the ITB phase for shot no. 69670 at $\rho = 0.30$. The v_θ profile for $0.55 < \rho < 0.80$ (radial width of 17 cm) is almost flat at

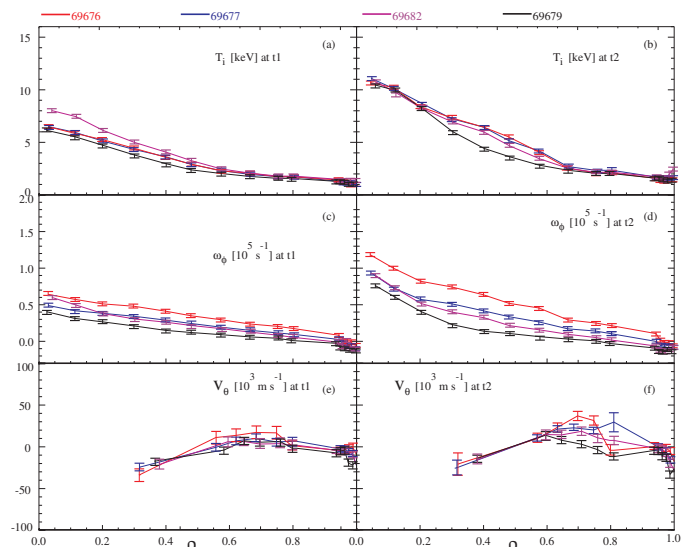


Figure 2: (a-b) ion temperature, (c-d) toroidal and (e-f) poloidal rotation velocity for the series of four OS shots with different ripple amplitude, before the start of the ITB on the left hand side, and around the maximum of the ITB strength on the right hand side for the times indicated in table 2

t_1 , but spins up to between 35 and 75 km/s in positive direction at t_2 , with the peak value at the foot of the ITB. In fig. 2 the equivalent profiles to those in fig. 1 are depicted for OS scenario. Generally the OS ITBs are weaker. Similarly to the RS cases the ITB strength decreases with increasing δ , and the edge v_θ shows a counter rotating zone that extends further inwards with increased ripple. The v_θ profiles at t_1 are relatively similar to the profiles for the RS shots before the ITB phase. No spin-up in the negative direction is observed around $\rho=0.30$ at t_2 . At the foot of the ITB the maximum v_θ is 40 km/s for $\delta=0.08\%$ and 15 km/s for $\delta=1.00\%$.

RADIAL ELECTRIC FIELD

Measured v_θ profiles for carbon impurities for shots 69665 and 69677 are plotted in figures 3 (a) and (b) respectively as well as the neoclassical predictions by the NCLASS module in the JETTO code. The v_θ measurements are limited to the radial region $\rho > 0.3$ and were set to zero for $\rho < 0.3$. It can

be seen that the measured v_θ is very different from the neoclassical prediction

for main and impurity ions in the ITB region, confirming previous results on JET [7]. The E_r profiles are plotted in figures 3 (c) and (d), calculated using the force balance equation for

carbon impurity ions: $E_r = \frac{1}{Zen_Z} \frac{dp_Z}{dr} - v_\theta B_\phi + v_\phi B_\theta$ (1), where Z is the impurity ion charge

number, e the electron charge, p_Z the impurity pressure and n_Z the impurity density, B_θ is the poloidal and B_ϕ the toroidal magnetic field. Due to the relatively large importance of the $(-v_\theta B_\phi)$ term, the E_r profiles are strongly affected by the high v_θ in the ITB region. A strong gradient in E_r is observed in the region $\rho=0.3-0.5$ when using the experimental values instead of the neoclassical predictions. The individual terms from eq. (1) and the total E_r are plotted in fig. 4. The pressure gradient is the weakest contribution. The toroidal rotation term is largest for the no-ripple case and decreasing with increasing δ . The largest contribution to the total E_r

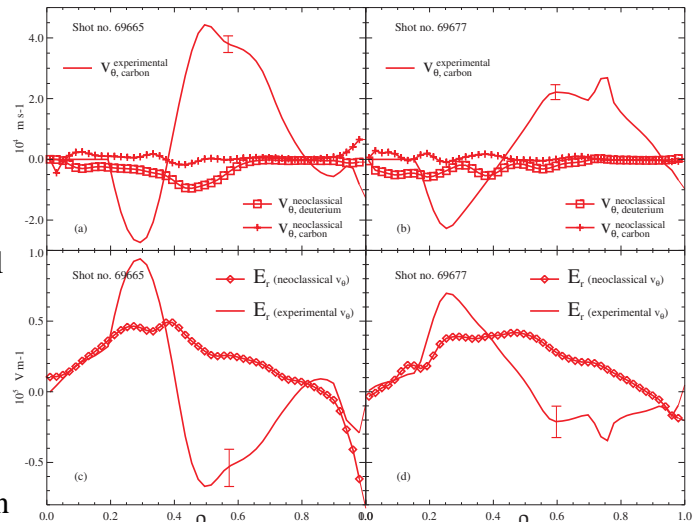


Figure 3: (a) and (b) experimental v_θ and neoclassical predictions by NCLASS for main ions and carbon impurities at t_2 (c) and (d) E_r profiles using the experimental and neoclassical v_θ . Typical error bars are shown on the experimental profiles.

is caused by the strong v_θ in the region with strong T_i gradient $0.20 < \rho < 0.75$. The largest v_θ is observed for the strongest ITBs (shots 69670, 69665 and 69676, 69677). For the weaker barriers (shots 69684, 69690 and 69682, 69679) the contribution from v_θ also dominates the shape of the total E_r . These observations indicate that the amplitude of v_θ is linked to the strength of the ITB and plays a significant role in the rotational shear. The maximum v_θ decreases with increasing TF ripple amplitude, but cannot be separated from the accompanied decrease in ITB strength. From the present dataset it is not clear whether the ripple effects v_θ directly or through ρ^*_{Ti} . In all shots the radial region with strongest T_i gradient coincides with the strongest E_r gradient.

CONCLUSIONS

ITBs are triggered in both RS and OS scenarios, but grow stronger in the RS case, when also the total E_r is strongest. Large TF ripple leads to weaker barriers. Toroidal rotation profiles are directly affected by the ripple, for $\delta=1.00\%$ a radial layer of about 20 cm is counter rotating. Stronger barriers are associated with the occurrence of an increased v_θ . Increasing δ leads to lower values of v_θ , but also decreases the maximum ρ^*_{Ti} . The measured v_θ is up to 20 times larger than the neoclassical predictions and contributes more than 50% to the total E_r and shearing rate, which is believed to break up turbulent eddies and reduce transport.

Acknowledgments

This work, carried out under the European Fusion Development Agreement, supported by the European Communities and Royal Military Academy (RMA), Belgium, has been carried out within the Contract of Association between EURATOM and the Belgian State. Financial support was also received from Ghent University (UG), Belgium. The views and opinions expressed herein do not necessarily reflect those of the European Commission, RMA and UG.

References

- [1] H. Urano et al., Nucl. Fusion (2007), Vol. 47, 706-713
- [2] P.C. de Vries et al., Nucl. Fusion (2008), Vol. 48, 035007
- [3] P.C. de Vries et al., Plasma Phys. Control. Fusion (2008), Vol. 50, 065008
- [4] G. Tresset et al., Nucl. Fusion (2002), Vol. 42, 52
- [5] C. Negus et al., Rev. Sci. Instrum. (2006), Vol. 77, 10F102
- [6] Y. Andrew et al., Rev. Sci. Instrum. (2006), Vol. 77, 10E913
- [7] K. Crombé et al., Phys. Rev. Lett. (2005), Vol. 95, 155003

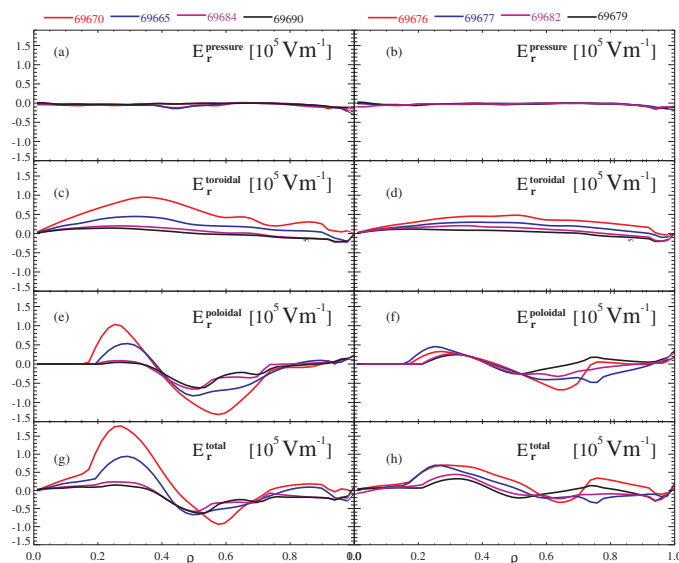


Figure 4: Different contributions to E_r : (a-b) Pressure gradient term ($1/Zen * dp/dr$), (c-d) toroidal rotation term ($v_\theta B_\theta$), (e-f) poloidal rotation term ($-v_\theta B_\theta$), (g-h) total E_r .